

Project Title:**Computational Studies of Muon Locations, Electronic Structures and Electron Transport in High- T_c Superconductor, Organic, Organometallic and Biological Systems.****Name:**

○Shukri Sulaiman (1,2), Isao Watanabe (2), Dita Puspita Sari (2,3), Muhammad Redo Ramadhan (2,4), Irwan Ramli (2,5), Wan Nurfadhilah Zaharim (1,2), Peter Greimel (2), Supparat Charoenphon (2,6)

Laboratory at RIKEN:

- (1) Universiti Sains Malaysia, Malaysia
- (2) RIKEN, Nishina Center, Japan
- (3) Shibaura Institute of Technology, Japan
- (4) Universitas Indonesia, Indonesia
- (5) Hokkaido University, Japan
- (6) Kasetsart University, Thailand

1. Background and purpose of the project, relationship of the project with other projects

i High- T_c superconducting oxides

a. La_2CuO_4

The mother material of the La-based high- T_c superconducting oxides, La_2CuO_4 (LCO), is the typical Antiferromagnetic Mott insulator. LCO has been well investigated experimentally and theoretically in the past, but there are still questions on electromagnetic states. Those are the on-site Coulomb potential, U , and the covalent state of the electronic orbitals of Cu. The muon spin resonance technique (μSR) can provide information on local magnetic fields at the muon site. It is very difficult to obtain the muon effect in the structure. Our attempt to solve the problem within the density functional theory (DFT) framework has yielded mixed results. More specifically, the local-spin-density approximation (LSDA) and the generalized gradient approximation (GGA) incorrectly predict La_2CuO_4 to be nonmagnetic (NM) metals in complete disagreement with the experimental value. Due to the self-interaction error (SIE), local and semi-local functionals systematically underestimate band gaps, occasionally to the extent that semiconductors are erroneously predicted to be metallic. DFT+U has

found favor as a method that strikes a reasonable balance between accuracy and computational cost, making it particularly suitable for high-throughput computation DFT+U functionals add a correction to the conventional XC functional to account for the Coulombic interaction between localized electrons. The DFT + U (local density approximation (LDA) + U and generalized gradient approximation (GGA) + U) approach has been shown to effectively correct many of the deficiencies observed in this class of materials with regards to the band gap. On the other hand, the development of methods, which incorporate stronger electron correlations to stabilize the AFM ground state, has effectively described the low-energy spectra of the cuprates. The meta-GGA exchange-correlation (XC) function improves upon a generalized gradient approximation (GGA). The most successful meta-GGA is SCAN, the strongly constrained and appropriately normed (SCAN), which obeys all known constraints applicable to a meta-GGA functional. SCAN is the only density functional that correctly predicts the band gap and the magnetic moments of the undoped cuprate high-temperature superconductor materials without free parameters. In this work, we apply the DFT+U (GGA+U and LSDA+U) and SCAN functional to investigate the detail of the ground-state electronic

structure surrounding the muon and the muon localization site to compare with the experiment value from the muon spin resonance technique (μ SR).

b. $\text{La}_{2-x}(\text{Sr}_x, \text{Ba}_x)\text{CuO}_4$

High temperature superconducting cuprate (HTSC) is known to have fascinating properties, such as pseudogaps, stripe of spins and holes, unconventional normal states, and charge-ordered states. Those unique features are usually realized with the idea of strong on-site Coulomb potential, U , and the covalent states of Cu 3d orbitals with the surrounding O 2p orbitals. To understand more regarding the effect caused by the on-site Coulomb potential of U , mother compound of the HTSC, La_2CuO_4 (LCO) can provide an ideal playground.

The value of U on the Cu atom has been well investigated but still has large ambiguities between 3-10 eV, resulting on uncertainty on the discussion about the unique features HTSC have. Following this we suggest an approach to this problem by combining muon spin rotation (μ SR) technique with density functional theory (DFT) calculation including U as an adjustable parameter (DFT+ U)

In the current computational project, we have already determined some symmetric positions and its effect to the internal field at $U = 5$ eV by assuming both point dipole spin and distributed spin. Finally, we conclude our study by fitting the difference of internal field and utilized U values.

iii Study on the λ -(D) $_2\text{GaCl}_4$ [$D = \text{BEST}, \text{ET}, \text{STF}$] sister compounds

The organic superconductor λ -($\text{BETS})_2\text{GaCl}_4$ [$\text{BETS}=(\text{CH})_2\text{S}_2\text{Se}_2\text{C}_6\text{Se}_2\text{S}_2(\text{CH}_2)_2$] is an unconventional superconductor. The so-called distorted nodal line was reported in the previous report from our μ SR experiment, and we revealed from the DFT calculation the detail structure of the distorted Fermi surface in λ -($\text{BETS})_2\text{GaCl}_4$, owing to its lattice which is an anisotropic triangular

alternating with squared lattice. To investigate the mechanism of superconductivity in λ -($\text{BETS})_2\text{GaCl}_4$ the relationship between superconducting (SC) and adjacent electronic phases by physical or chemical pressure effect are worth to study. The chemical pressure effect of substituting bromine for chlorine in 1 -($\text{BETS})_2\text{GaCl}_4$ has been studied. However, in the system of λ -($\text{BETS})_2\text{GaBr}_x\text{Cl}_{4-x}$, the pressure range investigated by bromine substitution is narrow because 1 -type salts can be obtained only in the range $x < 2$ and superconductivity occurs at 0.12 GPa for $x = 1.5$.

For complementary information on a wider pressure range, a universal phase diagram using donor molecular substitution has been proposed, as illustrated in Figure 1. The D site is changed from BETS containing Se and S to the ET reducing the Se contents. The negative pressure effect can be drawn and eventually an antiferromagnetic phase region emerged in the vicinity of superconducting phase although a peculiar paramagnetic phase is sandwiched between them. We continue the μ SR study on these compounds. On the other hand, although rich phase diagram of several phases emerged, all the families have an almost isostructural crystal structure.

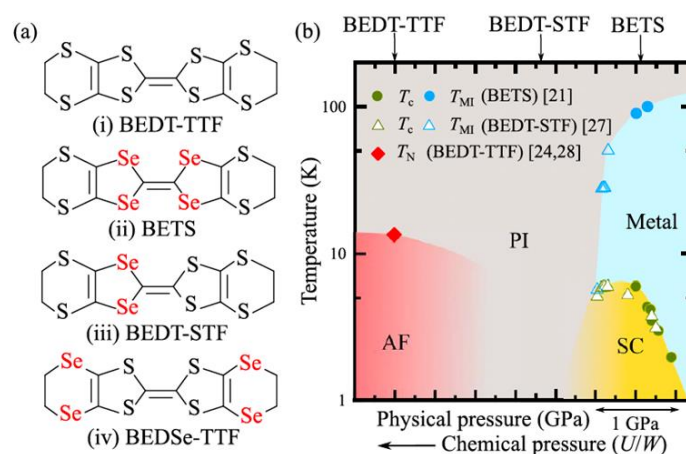


Figure 1. (a) Molecular structures of (i) BEDT-TTF, (ii) BETS, (iii) BEDT-STF, and (iv) BEDSe-TTF. (b) Phase diagram of 1 -(D) $_2\text{GaCl}_4$ ($D = \text{BEDT-TTF}, \text{BEDT-STF}, \text{BETS}$), adopted from our report listed in the List of publication.

iv Study on the κ -(ET)₄Hg_{2.89}Br₈

The hole-doped organic superconductor κ -(ET)₄Hg_{3-d}Br₈, $d=11\%$ (κ -HgBr) has been the key to bridge the knowledge between half-filled organics and doped cuprates system, as the well-known Mott-Hubbard model in the laboratory. Usually, the organics superconductivity appears under pressure when the ratio of Hubbard interaction and bandwidth, U/W , is less than 1. Nonetheless, the triangular lattice of organics, unlike the squared lattice in the cuprates, provides an extensive

geometrically control through nearest, t , and next nearest, t' , transfer integral between sites. In the

case of geometrically triangular frustration ($t \sim t'$),

the Mott insulating state cannot be magnetically ordered down to the milli-Kelvin (mK) order, becoming a Mott quantum spin liquid. Specifically, both hole-doped superconductors have some region of the strange metallic state at which resistivity exhibits the linear-temperature dependence,

$\rho \propto T$, which is not a Fermi-liquid (non-FL) behavior.

Our ZF- μ SR experiment showed that the time reversal symmetry is preserved in the superconducting state of κ -HgBr down to 0.3 K narrowing the similarity down to that of cuprates despite the triangular lattice. Furthermore, we confirmed that there is a relatively large changing of the relaxation rate seen from the ZF- μ SR from 300 to 100 K before the curve shape changing, shown in Figure 2. It is suspicious that muon is probably hopping. The support from theoretical calculation is necessary to discuss the behavior of the relaxation rate at wide temperature region.

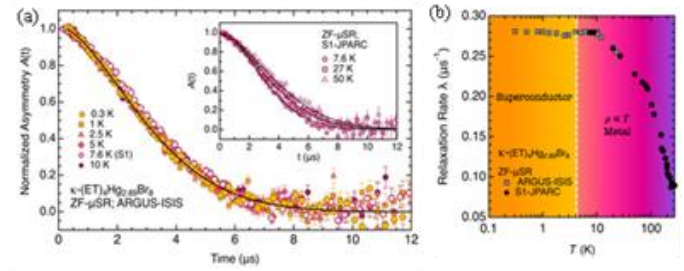


Figure 2. The ZF- μ +SR time spectra upon ZF-cooling in κ -HgBr. (a) Yellow and pink symbols are the ZF- μ +SR spectra measured at wide temperature range crossing $T_c = 4.6(2)$ K down to 0.3 K. The data taken at 300 – 7.6 K were measured on S1, JPARC facility, whilst those taken at 10 – 0.3 K were measured on ARGUS, ISIS facility. (b) Temperature dependence of ZF- μ +SR relaxation rate $\lambda(T)$ deduced from the solid lines in (a).

v Magnetic Ordering and Origin of Metal-Insulating Transition of Eu₂Ir₂O₇

Pyrochlore iridate, Ln₂Ir₂O₇, with Ln is lanthanide have interest properties in which its metal insulator transition strongly depends on Ln radius. The lanthanide elements have trivalent ions, in which the $[(5d)]^5$ electrons of Ir⁽⁴⁺⁾ form an unfilled t_{2g} band, in this case only the lanthanide elements which have 5d electrons can exhibit electrical conductivity. The compounds from the lanthanide Pr were identified as having no MIT up to 0.3K, while identification using the Kondo effect at $T_k=25k$ with a strong c-f hybridization effect showed that the ionic radius limit for MIT (Ln₂Ir₂O₇) was between Ln=Pr and Nd. Ln₂Ir₂O₇ for Ln=Nd, Sm, and Eu have MIT of 36K, 117K, and 120K respectively. Eu₂Ir₂O₇ has attracted particular attention because it not only exhibits a strong MI transition, it also offers the advantage of nonmagnetic of Eu³⁺ ion spin (S) and orbital angular momentum (L) complement each other. Therefore, the magnetism and related topological properties arise solely due to the 5d electrons of Iridium. The magnetic ordering and its

magnetic moment size still debatable for this system. We study $\text{Eu}_2\text{Ir}_2\text{O}_7$ by muon spin resonance to investigate its magnetic properties and spin dynamic. This technique has limitation due to unknown of muon position and the perturbation of muon. We address this issue by density functional theory(DFT) calculation to search the minimum potential as initial position of implanted muon and put artificial muon in this position to study the muon's perturbation to the system.

As first state, we study the effect of hubbard parameter, spin-orbit Coupling and magnetic ordering in this system. We calculate the band structure and density of state (DOS) by considering Hubbard U and Spin Orbit Coupling. After we got realistic results, we will search for the muon position within unit cell.

vi Single and double strand 12mer synthetic DNA oligomers

Electron transport is involved in many important biological processes, including energy storage and consumption, enzyme response, and DNA UV damage repair. μSR is an experimental method for studying electron transport phenomena in DNA at the microscopic level. Changes in electron transport properties caused by DNA damage can be investigated using muon hyperfine interactions, which are extremely sensitive to changes in the electronic structure surrounding the muonium (Mu) trapping sites. To systematically study the effect of DNA damage on electron behavior, it is critical in developing baseline data using DNA systems with known DNA sequences.

The Mu hyperfine interactions at all possible Mu trapping sites in the four nucleobases, four nucleotides, and four homogenous single-strand DNA oligomers were investigated in a previous project. For the nucleobase and nucleotide molecules, the results show that adding a methyl group or a sugar-phosphate group to the nucleic acid bases has a direct effect on the system's electronic structure.

The geometry of guanine nucleobase was tested for distortion when Mu was added to the possible trapping sites. The optimized muoniated systems structure was examined to see if the presence of Mu caused the guanine base ring to deviate from its planar shape.

Thus, in FY2022, 12mer single-strand DNA with homogeneous nitrogenous bases was chosen as a model for this study. In this investigation, we performed DFT calculations to determine the geometry, electronic structure, and molecular properties, as well as Mu trapping sites, in 12mer ssA, 12mer ssC, and 12mer ssT oligomers.

2. Specific usage status of the system and calculation method

The Gaussian16 and Vienna Ab initio Simulation Package (VASP) software packages are the two main ab initio quantum mechanical programs used in this group. The Gaussian program package is more suitable for the electronic structure studies of molecular systems because it employs the linear combination of atomic orbital molecular orbital (LCAO-MO) technique. The VASP software, on the other hand, has been used in band theory calculations for solid systems as it employs pseudopotentials or the projector-augmented wave method and a plane wave basis set. Furthermore, the ADF software was used in our computational work to provide improved results on the hyperfine coupling constant (HFCC). Next, NBO for Gaussian is used in this project, which is based on a method for optimally transforming wave functions into localized form. MATLAB is a high-performance language for technical computing that integrates computation, visualization, and programming in an easy-to-use environment. Wannier90 was also used in this project. It is an open-source code for generating maximally localized Wannier functions and using them to compute advanced electronic materials with high efficiency and accuracy. It is proven that the HOKUSAI Great Wave supercomputer facility is

crucial and extremely useful for our group research, particularly for large-scale calculations due to the results obtained from the calculations by using all the resource units.

3. Result

In section 1, a considerable amount of computational effort has been done in FY2022 on the different systems described. The data from the computational studies is collected to assist the interpretation of μ SR experiments. The results for each subproject are reported separately and are as follows:

i High-Tc superconducting oxides

a. La_2CuO_4

- Fundamental properties of La_2CuO_4

The lattice parameter calculated by LSDA+U, GGA+U and SCAN, band gap, and magnetic moment are listed in Table 1. The calculated lattice parameters are in very good agreement with the experimental values. Our calculated bandgap of La_2CuO_4 are 0.8110 , 0.9771 and 1.007 eV for LSDA+U , GGA+U and SCAN, respectively.

Table 1 Calculation of structural parameter, band gap, and magnetic moment of a unit cell of La_2CuO_4 .

- Muon stopping site in La_2CuO_4

Next step, the LSDA+U, GGA+U, and SCAN were carried out, including the muon, to reproduce the μ SR results. We estimate the initial position of muon injection in La_2CuO_4 obtained from the electrostatic potential shown in Figure 3(a). There are three possible local minimum potential positions that muon can stop in the structure, which are M1, M2, and M3, compared with the μ SR results. The final muon position and local deformations of the crystal structure estimated from our DFT+ μ calculation show the final position of M1, M2, and M3 in the same position in different functions. Still, the magnetic moment and electrostatic position of Cu and O atoms around muon are different, shown in

Figures 3(b), 3(c), and 3(d), respectively.

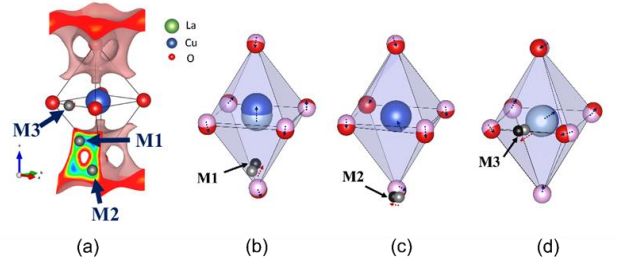


Figure 3 (a) Electrostatic potential calculation result. The grey sphere indicates three local-minimum potential positions as candidates for initial muon-stopped positions. (a) show the final muon position after relaxation for (b) M1, (c) M2, and (d) M3, respectively. The Grey sphere represented the initial position. The black sphere represented the final position of the muon after the relaxation.

b. $\text{La}_{2-x}(\text{Sr}_x, \text{Ba}_x)\text{CuO}_4$

Table 1. Calculated magnetic moment of the Cu-spin without muon by varying U, and the calculated internal field at M1, M2, and M3 position

| U (eV) | Mag. Moment (μ_B) | H_{M_1} (G) | H_{M_2} (G) | H_{M_3} (G) |
|-------------|-------------------------------|------------------|------------------|------------------|
| 2 | 0.386 | 336.35 | 103.99 | 888.06 |
| 3 | 0.436 | 376.01 | 116.30 | 990.60 |
| 3.5 | 0.460 | 384.85 | 121.28 | 1038.67 |
| 4 | 0.482 | 391.51 | 127.04 | 1077.89 |
| 4.5 | 0.503 | 429.98 | 131.21 | 1128.28 |
| 5 | 0.524 | 446.36 | 135.68 | 1169.74 |
| 5.6 | 0.547 | 450.22 | 141.54 | 1219.72 |
| 6 | 0.562 | 471.50 | 145.85 | 1241.02 |
| 6.5 | 0.583 | 474.90 | 150.14 | 1281.64 |
| 7 | 0.602 | 491.08 | 154.33 | 1322.98 |
| 7.2 | 0.609 | 503.83 | 155.44 | 1334.41 |
| 7.5 | 0.621 | 507.16 | 159.07 | 1364.36 |
| 8 | 0.641 | 523.10 | 163.76 | 1407.01 |

Table 1 shows the the calculated internal field variation on three muon position. Based on this data, we defined the differences between calculated internal field and experimental internal field by following the equation:

$$\Delta H_{M_i} = (H_{\text{DFT}}^{M_i} - H_{\mu\text{SR}}^{M_i}), \quad (i = 1,2,3)$$

After that, we summed up all ΔH_{M_i} for each U with fitting error values from internal fields, σ_i :

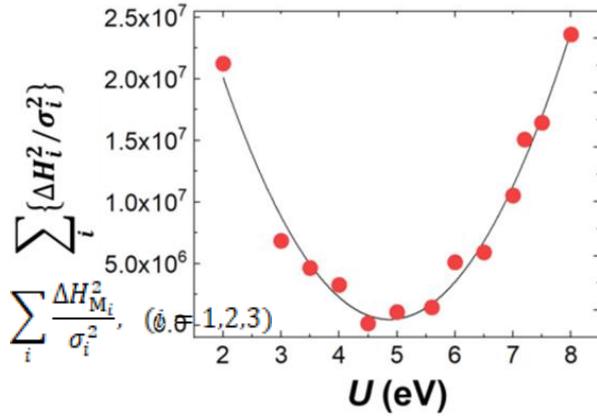


Figure 4. Optimization U in terms of the difference of internal field obtained by μSR and DFT+U calculations. The solid line is the best-fit result by using Gaussian function

Figure 4 shows the U-dependence of summed up values obtained from the equations. By applying the Gaussian function, U was optimized to be 4.87(4) eV. This values locates at the lower end of the U range which has been argued to be from 3 to 10 eV as described in the background study. This U value will produce charge transfer gap value of 1.24(1) eV and magnetic moment value of 0.520(3) μ_B

We also considers the symmetric position to the calculated internal field. Here we consider same supercell and calculation's condition and fixing the U to be 5 eV. Table 2 shows the the Cartesian coordinates of M1 positions and 2 of its symmetric positions.

Table 2. Cartesian position of M1 and its symmetric position after relaxing the supercell structure and magnetic moment of nearest Cu-atom to the muon.

| | a | b | c | D-Cu _{nearest} | Mag. |
|------|---------|---------|---------|-------------------------|-------------|
| | | | | (Å) | Mom. |
| | | | | | (μ_B) |
| M1 | 0.37774 | 0.61744 | 0.43747 | 1.87862 | 0.498 |
| M1' | 0.37303 | 0.61685 | 0.43686 | 1.88868 | 0.498 |
| M1'' | 0.37678 | 0.61707 | 0.43689 | 1.88678 | 0.497 |

From this data we can see that even changing the initial position to its symmetric position within local structure of Cu-O, the relaxed position always goes to the position which have similar distance to the nearest Cu atom ($\sim 0.5\%$ differences). The differences could be due to the accuracy limit of convergence criteria that we set (atomic force between atom should be lower than 0.05 eV/Å). We also obtain that the magnetic moment of the nearest Cu atom is similar ($\sim 0.2\%$ differences). By calculating the internal field based on the assumption of point dipole spin and considering the local deformed supercell structure we obtain that the difference between three symmetric position is $\sim 0.25\%$. If we consider the distributed spin model, the differences between symmetric position is $\sim 2\%$. The difference (between point spin and distributed spin) is caused by the fact that distributed spin model is more sensitive to the difference of muon position. Furthermore, this value is also limited by the force convergence criteria that we set (0.05 eV/Å).

iii Study on the λ -(D)₂GaCl₄ [D = BEST, ET, STF]
The zero-field (ZF) μSR experiment was recently done in λ -(BEDSe-TTF)₂GaCl₄, which showed an antiferromagnetic ground state. To discuss the experiment in detail, we performed the muon stopping site calculation. Figure 5 show the ZF- μSR time spectra of λ -(BEDSe-TTF)₂GaCl₄ which was best fitted using two oscillation components B_{μ1} and

$B_{\mu 2}$ of the muon spin precession. The plot of $B_{\mu 2}$ against $B_{\mu 1}$ shown in Figure 5 indicates that they are proportional to each other. The temperature evolution of the $B_{\mu 2}$ and $B_{\mu 1}$ is shown in Figure 5. These results strongly suggests that the two observed rotational components correspond to the muons stopped at magnetically inequivalent sites. And that the development of the magnetic moment is observed from different muon site.

We discuss the positions of the two muon sites from the density functional theory (DFT) calculation performed within Kohn-Sham approach using the projector augmented-waves formalism in the VASP program. The exchange-correlation function generalized gradient approximation, GGA-PW91, was used. The ground-state charge densities were calculated by adopting the value of the crystal axis determined by the X-ray diffraction measurement, and by using the $4 \times 4 \times 4$ k -point sampling, ultrasoft pseudopotentials, and plane-wave densities. Figure 6 shows the crystal structure of λ -(BEDSe-TTF) $_2$ GaCl $_4$ and the electric minimum potential with the isosurface of 37.8 eV shown in cyan. Although there are several possible muon sites, we found two major sites: $M1$ near GaCl $_4$, and $M2$ near the ethylene groups. If the spin density is larger near the ethylene edge, it is likely that $M1$ and $M2$ are related to $B_{\mu 1}$ and $B_{\mu 2}$, respectively. Although λ -BEDSe has a complex crystal structure, the major two muon sites observed in the present study can be consistently explained by the DFT calculations. This result is reported in journal Physical Review B and listed in the List of Publication section of this report.

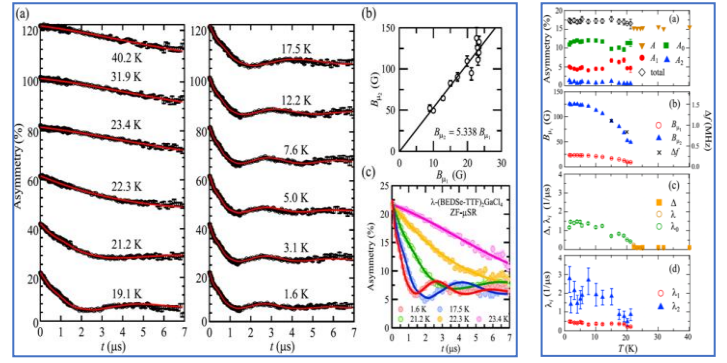


Figure 5 (left) (a) Temperature evolution of μ SR time spectra at zero magnetic field. (b) Relationship between $B_{\mu 1}$ and $B_{\mu 2}$ with the linear fitting. (c) Representative μ SR time spectra with the fitting using $B_{\mu 2} = 5.338 B_{\mu 1}$. (right) Temperature dependence of the parameters obtained by fitting the μ SR time spectra showing the temperature dependence of the two oscillation components in (b)

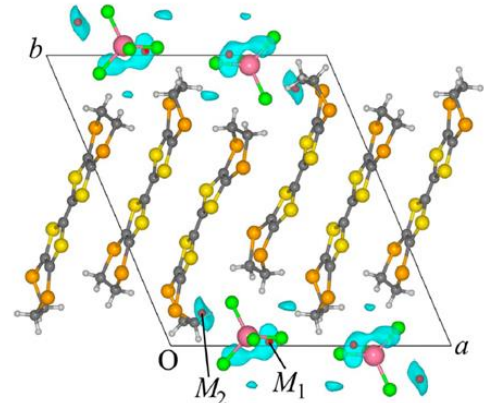


Figure 6. Crystal structure of λ -(BEDSe-TTF) $_2$ GaCl $_4$, and electric minimum potential with isosurface of 37.8 eV shown in the cyan region. The most possible muon stopping sites are marked in red.

iv Study on the κ -(ET) $_4$ Hg $_{2.89}$ Br $_8$

To discuss a relatively large changing of the relaxation rate seen from the ZF- μ SR from 300 to 100 K before the curve shape changing, shown in Figure 7. The support from theoretical calculation is necessary. We discuss the positions of muon sites from the density functional theory (DFT) calculation performed within Kohn-Sham approach using the projector augmented-waves formalism in the VASP program. The exchange-correlation function generalized gradient approximation, GGA-PW91,

was used. The ground-state charge densities were calculated by adopting the value of the crystal axis determined by our X-ray diffraction measurement, and by using the $6 \times 5 \times 2$ k -point sampling, ultrasoft pseudopotentials, and plane-wave densities. Figure 2.ii show the crystal structure of κ -(ET)₄Hg_{2.89}Br₈, and electronic minimum potential with isosurface of 75 meV, 135 meV, 200 meV. The possible muon stopping sites are shown by the blue arrows. It is understandable that the lowest minimum potential energy is shown by the isosurface 75 meV. The second lowest one is shown by the isosurface 135 meV. Then, the third one is shown by the isosurface 200 meV. This means in order muon to hop to the next minimum potential energy it is required energy in the range as high as 1450 K to 700 K. Therefore, the DFT calculation supported that the relatively large changing in the relaxation rate at 100 – 300 K is not due to the muon hopping.

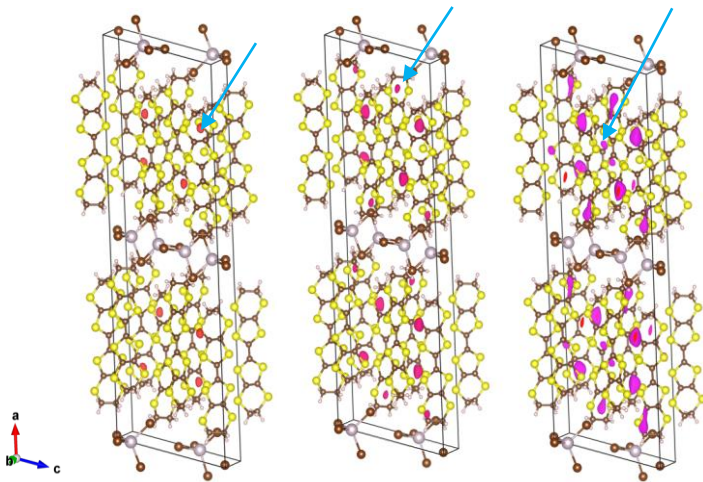


Figure 7 Crystal structure of κ -(ET)₄Hg_{2.89}Br₈, and electronic minimum potential with isosurface of 75 meV, 135 meV, 200 meV, shown from the left side figure to the right-side figure, with purple, magenta, and red color respectively. Blue arrows indicate the possible muon stopping site from the lowest energy to the 2nd and 3rd lowest energy from left to the right-side figure, respectively.

v Magnetic Ordering and Origin of Metal-Insulating Transition of Eu₂Ir₂O₇

The calculations of the electronic properties of

pyrochlore Eu₂Ir₂O₇ by DFT was carried out with 4 different schemes. The first scheme is performed without hubbard correction (U=0) and without SOC, the second scheme is carried out by adding corrections hubbard (U=1.3 eV) and without SOC, the third scheme using SOC and without Hubbard and fourth scheme is considering both hubbard correction (U=1.3 eV) and SOC. The results of electronic band structure calculations without hubbard correction (U=0) and SOC show that pyrochlore Eu₂Ir₂O₇ has a fermi energy of 12.5465 eV. Whereas in the second model the electronic bands structure and DOS calculations are added with hubbard correction (U=1.3 eV) without SOC indicating that the pyrochlore Eu₂Ir₂O₇ has a fermi energy of 12.5205 eV and in the third model the electronic bands structure and DOS calculations use hubbard correction and SOC shows a fermi energy of 12.5460.

All of our calculation scheme calculation models also show that there is no gap between the valence band and the conduction band or zero band gap which indicates that pyrochlore Eu₂Ir₂O₇ is metallic. In the electronic band structure of pyrochlore there is also a dirac cone or a conical meeting point between the valence band and the conduction band. This Dirac point shows that pyrochlore has an electron-electron interaction that induces a Weyl semimetal phase. Pyrochlore Eu₂Ir₂O₇ has a strong Spin-Orbit Copling (SOC), and the interaction between SOC and electron-electron correlation (U) will produce a unique electronic state, where the Eu₂Ir₂O₇ electronics experience isolation which is marked by the presence of a Metal Insulator Transition (MIT).

On the Density of States (DOS) graph there are energy levels that pass through the Fermi energy indicating metallic properties. From the results of electronic band structure and DOS calculations, it can be seen that the electronic properties of pyrochlore Eu₂Ir₂O₇ from our calculation is conductors. We still need to tuning some parameter to produce a weyl semimetal as first step to

understand the origin of MIT.

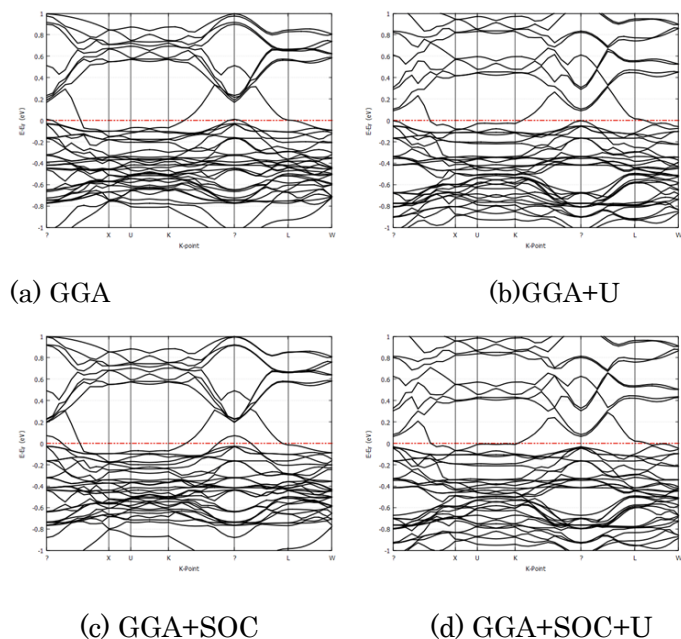


Figure 8. Band structure of $\text{Eu}_2\text{Ir}_2\text{O}_7$ (a) GGA, (b) GGA+U, (c) GGA+SOC, (d) GGA+SOC+U

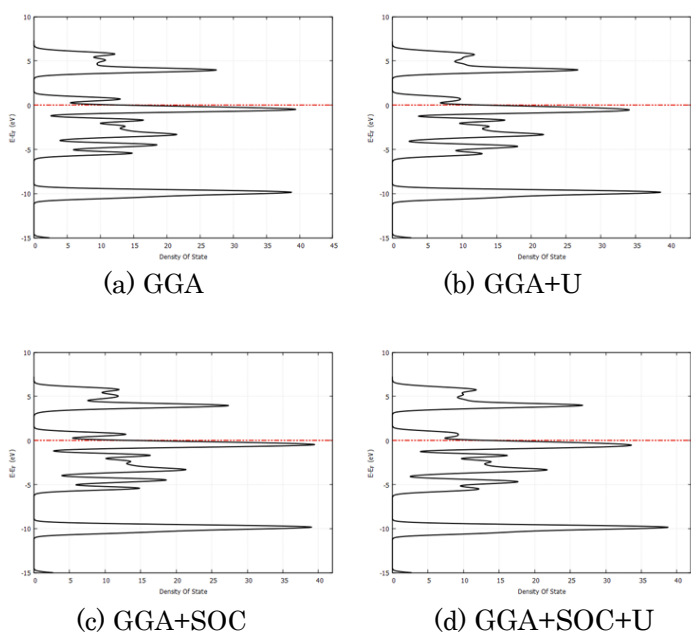


Figure 9. Density of State of $\text{Eu}_2\text{Ir}_2\text{O}_7$ (a) GGA, (b) GGA+U, (c) GGA+SOC, (d) GGA+SOC+U

vi Single and double strand 12mer synthetic DNA oligomers

Here we report our published data on the DFT study on muoniated short single-strand DNA molecules. The total number of possible Mu trapping sites in 12mer ssG, 12mer ssA, 12mer ssC, and 12mer ssT oligomers that were investigated in this work is 96, 96, 72, and 72, respectively. Figure 10, Figure 11,

and Figure 12 show the scatter plot of relative energies and $|\mu\text{on HFCCs}|$ of 12mer ssA, 12mer ssC, and 12mer ssT oligomer Mu trapping sites respectively.

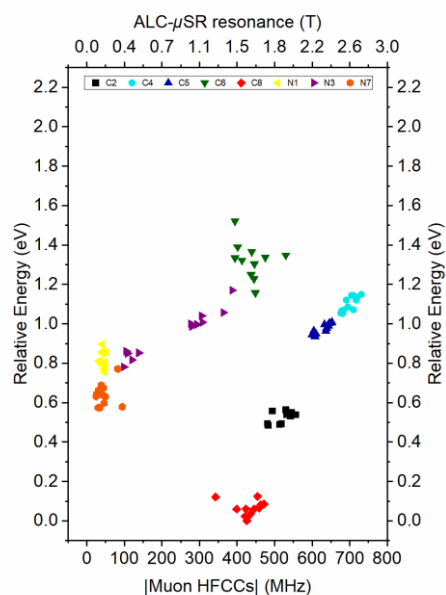


Figure 10. Scatter plot of relative energies and $|\mu\text{on HFCCs}|$ of 12mer ssA oligomer Mu trapping sites.

For 12mer ssA, C8-A-B12 has the lowest total energy, which is $-452,251.343$ eV. The relative energies of the 96 sites lie in the range of 1.521 eV. The Mu site with the highest energy is C6-A-B4. All 12 C8 sites have lower energies than the other Mu sites in the 12mer ssA oligomer. The calculated muon HFCCs at C8 sites range from 342.6 MHz (C8-A-B7) to 471.8 MHz (C8-A-B4). The muon HFCCs for the remaining ten C8 sites are within this range. In the 12mer ssA oligomer, C2 is the second most stable Mu site. The muon HFCCs for all 12 C2 sites lie in the range from 480.8 MHz (C2-A-B3) to 556.1 MHz (C2-A-B10).

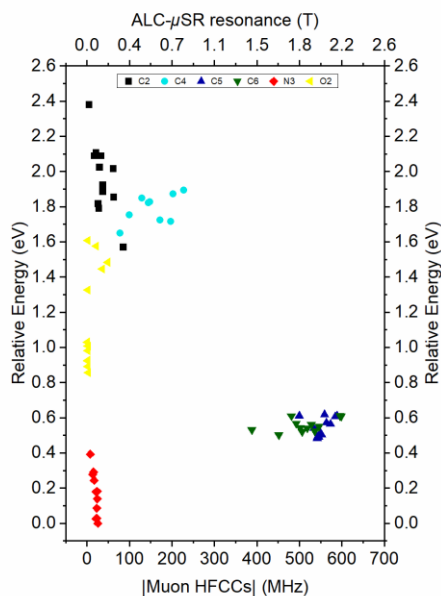


Figure 11. Scatter plot of relative energies and |muon HFCCs| of 12mer ssC oligomer Mu trapping sites.

For 12mer ssC, based on total energy, N3-C-B11 has the lowest total energy among the 72 sites, which is $-428,634.615$ eV. Among the 12 N3 sites, N3-C-B4 has the highest energy. The difference between the lowest and highest energy N3 trapping sites is 0.392 eV. The calculated HFCCs at N3 sites in 12mer ssC are in the range of -25.4 MHz (N3-C-B11) to -7.7 MHz (N3-C-B4). The next possible Mu stopping sites is C5 and C6. The calculated muon HFCCs at C5 sites range from 499.6 MHz (C5-C-B3) to 588.1 MHz (C5-C-B8). For C6 sites, the calculated HFCCs range from 387.8 MHz (C6-C-B2) to 598.7 MHz (C6-C-B8).

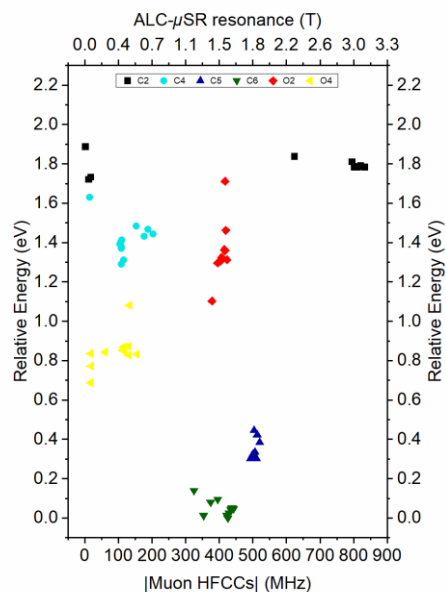


Figure 12. Scatter plot of relative energies and |muon HFCCs| of 12mer ssT oligomer Mu trapping sites.

For 12mer ssT, C6-T-B11 has the lowest total energy, which is $-447,953.699$ eV. All 12 C5 Mu sites have relative energy in the range of 0.301 eV (C5-T-B11) to 0.445 eV (C5-T-B4). Among the 12 C5 Mu sites, C5-T-B11 has the lowest energy, and it is 0.161 eV higher than C6-T-B2 (highest of all C6 sites). After C6 and C5, O4 sites are the next possible Mu trapping sites in terms of relative energy. Among the 12 O4 Mu sites, O4-T-B3 has the lowest energy, which is 0.687 eV higher than C6-T-B11 (lowest of all 72 Mu sites) and the Mu site with the highest energy is O4-T-B4, where the relative energy is 1.080 eV. The calculated HFCCs at C6 sites are in the range of 325.2 MHz (C6-T-B2) to 442.2 MHz (C6-T-B5). C5 sites have slightly higher Mu HFCCs as compared to C6 Mu sites, which are in the range of 493.5 MHz (C5-T-B11) to 520.9 MHz (C5-T-B1). The DFT calculated muon HFCCs at three sites, O4-T-B1, O4-T-B2, and O4-T-B3 are negative. The HFCCs values at these sites are -19.1 , -18.1 , and -18.1 MHz, respectively. For the other nine sites, the calculated Mu HFCCs are positive and in the range of 59.9 MHz (O4-T-B12) to 154.9 MHz (O4-T-B5).

4. Conclusion

i High-Tc superconducting oxides

a. La_2CuO_4

The band structure of La_2CuO_4 are 0.8110, 0.9771 and 1.007 eV for LSDA+U, GGA+U and SCAN, respectively. The GGA+U functional calculated the lattice parameter close to the experimental value compared to the LSDA+U and SCAN. On the other hand, the band gap was similar for GGA+U and SCAN within the experimental tolerance. For the muon stopping site calculation, the role of muon perturbation was found to deform the local crystal structure just around the muon. This effect leads to a slight reduction in the magnetic moment surrounding the muon.

b. $\text{La}_{2-x}(\text{Sr}_x, \text{Ba}_x)\text{CuO}_4$

We have successfully determine the value of U, the covalent state of Cu spin and the charge-transfer gap energy of LCO by combining μSR experiment and DFT calculation. Three muon positions are observed and U can be precisely determined to be 4.87(4) eV, the magnetic moment of Cu to be 0.520(3) μ_B , and the charge transfer gap value of 1.24(1) eV. We also consider the symmetric positions for muon and by considering both point spin and distributed spin model, we observed that the difference of calculated internal field are $\sim 0.25\%$ (point spin) and $\sim 2\%$ (distributed spin). Those differences are caused by the accuracy limit of our current calculation, where we set the force convergence criteria to be 0.05 eV/Å.

iii Study on the $\lambda\text{-(D)}_2\text{GaCl}_4$ [$D = \text{BEST, ET, STF}$] DFT calculation on the muon stopping site was successfully supported the μSR experimental result in $\lambda\text{-(BEDSe-TTF)}_2\text{GaCl}_4$, particularly the two oscillations component yielded from the ZF- μSR spectra. The antiferromagnetic ground state of the Mott insulating state can be concluded in the vicinity

of the peculiar paramagnetic and superconducting state of sister compounds. This result is important to obtain the universal phase diagram of the $\lambda\text{-(D)}_2\text{GaCl}_4$ family.

iv Study on the $\kappa\text{-(ET)}_4\text{Hg}_{2.89}\text{Br}_8$

The DFT calculation on the muon stopping site was successfully supported the μSR experimental result in $\kappa\text{-(ET)}_4\text{Hg}_{2.89}\text{Br}_8$ that the relatively large changing in the ZF muon relaxation rate at 100 – 300 K is not due to the muon hopping, since the difference between the lowest and second lowest minimum potential required the energy range as high as 1450 K to 700 K.

v Magnetic Ordering and Origin of Metal-Insulating Transition of $\text{Eu}_2\text{Ir}_2\text{O}_7$

We have calculated the electronic structure of $\text{Eu}_2\text{Ir}_2\text{O}_7$ as first step to understand the origin of MIT of $\text{Eu}_2\text{Ir}_2\text{O}_7$. We take in to account the Hubbard U and spin-orbit coupling. Our result show that $\text{Eu}_2\text{Ir}_2\text{O}_7$ is Metal. On the other hand, the experimental results show that $\text{Eu}_2\text{Ir}_2\text{O}_7$ is insulator. We suspect this discrepancy due to the magnetic ordering and we still need to tuning some parameters.

vi Single and double strand 12mer synthetic DNA oligomers

In this investigation, DFT calculations were performed to determine the geometry, electronic structure, and molecular properties, as well as Mu trapping sites, in 12mer ssA, 12mer ssC, and 12mer ssT oligomers. The possible Mu trapping sites were analyzed from the relative energy and HFCC value. The most probable Mu trapping sites in 12mer ssA oligomer are C8 and C2. For 12mer ssC, N3, C5, and C6 sites are the most stable Mu trapping sites 12mer ssT oligomer has three possible Mu sites, C6, C5, and O4. The distance between Mu and the ion which determines the strength of the hydrogen bond varies due to the relaxation effects of the atoms in the

proximity of μ .

5. Schedule and prospect for the future

i High-Tc superconducting oxides

a. La_2CuO_4

After we know the muon position, we must calculate the Effects of the Zero-Point Vibration Motion of μ and the internal field. The internal field at M1, M2, and M3 were calculated based on the dipole-dipole coupling and compared with the μSR time spectrum peak measured in the zero-field on the LCO single crystal.

Our DFT calculations were employed within the Generalized Gradient Approximation (GGA), and the pseudopotential projector augmented wave (PAW) method as implemented in the Vienna ab initio simulation package (VASP). We use a primitive cell to calculate the fundamental properties of $\text{Nd}_2\text{Ru}_2\text{O}_7$. A supercell structure containing 88 atoms was adopted for calculation, considering the effect of relaxations of muon position to compare with the experimental

b. $\text{La}_{2-x}(\text{Sr}_x, \text{Ba}_x)\text{CuO}_4$

Further investigation on whether it is possible to lower the force convergence criteria to be less than 0.05 eV/\AA , to establish the limit on how our technique (DFT+U+^U) should be applied on different systems. Obtain the effect of optimized U in LCO on the HTSC material such as La-Sr-Cu-O and La-Ba-Cu-O, for instance to its charge density and the density of states data.

iii Study on the λ - $(D)_2\text{GaCl}_4$ [$D = \text{BEST}, \text{ET}, \text{STF}$]

The muon stopping site calculation will be then extended to other sister compounds λ - $(\text{ET})_2\text{GaCl}_4$ and λ - $(\text{STF})_2\text{GaCl}_4$. Some of the electronic band structures have been indeed done for the λ - $(\text{STF})_2\text{GaCl}_4$ compound but not yet summarized in this report. We are in parallel still chasing the solid

result of the μSR experiment to carefully summarize the DFT and μSR results together. The λ - $(\text{STF})_2\text{GaCl}_4$ does not show the muon spin precession, making us more difficult to discuss μSR result in conjunction with DFT calculation. Further investigation both from DFT and experiment are necessary. Furthermore, we are continuing to calculate the transfer integral lattice like we have done in, λ - $(\text{BETS})_2\text{GaCl}_4$, for each compound and expect the systematic changing of the anisotropy of the lattice.

iv Study on the κ - $(\text{ET})_4\text{Hg}_{2.89}\text{Br}_8$

To study the superconducting mechanism in κ - $(\text{ET})_4\text{Hg}_{2.89}\text{Br}_8$, we as well study the sister insulating compound which has a different doping-content yet slightly higher U/W ratio than that of κ - HgBr , κ - $(\text{ET})_4\text{Hg}_{3-d}\text{Cl}_8$, $d=22\%$ (κ - HgCl for short). It shows metal-insulator transition at $T_M = 20 \text{ K}$ at ambient pressure. We plan to perform the DFT calculation to compare the muon stopping site since the μSR experiment on this sister compound has been started. The study of κ - $(\text{ET})_4\text{Hg}_{2.89}\text{Br}_8$ and κ - $(\text{ET})_4\text{Hg}_{3-d}\text{Cl}_8$ are supported by the KAKENHI grant 21K13885.

v Magnetic Ordering and Origin of Metal-Insulating Transition of $\text{Eu}_2\text{Ir}_2\text{O}_7$

For the future plan, we will calculate the potential map in $\text{Eu}_2\text{Ir}_2\text{O}_7$ to search the minimum potential as initial muon position within unit cell. Next calculations, we put muon at the initial position and relax the structure to see the effect muon to its surrounding. These calculations should be done in supercell. In the last step, we calculate the internal field by considering zero vibration motion of muon and compare with the existing experimental results.

iv Single and double strand 12mer synthetic DNA oligomers

The optimized structure of 12mer ssA, 12mer ssC, and 12mer ssT oligomers and the details information

Usage Report for Fiscal Year 2022

on the Mu trapping sites have been obtained and published. Thus, in the next fiscal year, we would like to obtain the electronic structure of short double-strand DNA molecules (dsGC, dsGC-CG, and dsGC-CG-GC) and their associate muon hyperfine coupling constant value.

6 . If no job was executed, specify the reason.

Fiscal Year 2022 List of Publications Resulting from the Use of the supercomputer

[Paper accepted by a journal]

1. Jamaludin, A., Zaharim, W. N., Sulaiman, S., Rozak, H., Ang, L.S., Watanabe, I. Density Functional Theory Investigation of Muon Hyperfine Interactions in Guanine-Cytosine Double-Strand DNA. *Journal of the Physical Society of Japan*, 91 (2022) 024301. (WOS indexed)
2. Zaharim, W. N., Sulaiman, S., Abu Bakar, S.N., Ismail, N.E., Jamaludin, A., Rozlan, A.F., Ang, L.S., Watanabe, I. Density Functional Theory Study of Muon Hyperfine Interactions in 12mer Single-Strand Adenine, Cytosine, and Thymine Oligomers. *Journal of the Physical Society of Japan*, 91 (2022) 094301. (WOS indexed)
3. Ramadhan, M. R., Adiperdana, B., Ramli, I., Sari, D. P., A. Putri, E., Widyaiswari, U., Rozak, H., Zaharim, W. N., Manaf, A., Kurniawan, B., Mohamed-Ibrahim, M.I., Sulaiman, S., Kawamata, T., Adachi, T., Koike, Y., Watanabe, I. Estimation of the on-site Coulomb potential and covalent state in La₂CuO₄ by muon spin rotation and density functional theory calculations. *Physical Review Research*, 4 (2022) 033044. (WOS indexed)
4. Ito, A., Kobayashi, T., Sari, D. P., Watanabe, I., Saito, Y., Kawamoto, A., Tsunakawa, H., Satoh, K., and Taniguchi, H., Antiferromagnetic Ordering of Organic Mott Insulator λ -(BEDSe-TTF)₂GaCl₄, *Phys. Rev. B*, 106 (2022) 045114. (WOS indexed)

[Oral presentation]

1. Charoenphon, S., Reunchan P., and Watanabe I. (November, 2022). Density Functional Theory Calculations with Different Electronic Correlational Functionals Applied to La₂CuO₄. *Oral presentation at the 6th International Conference on Functional Materials Science (ICFMS 2022)*. Bali, Indonesia.
2. Charoenphon, S., Reunchan P., and Watanabe I. (January, 2023). Density Functional Theory Calculations with Different Electronic Correlational Functionals Applied to La₂CuO₄. *Oral presentation at the muon meeting*. RIKEN, Saitama, Japan.

[Poster presentation]

1. Sari, A., Nurfalaq, A., Watanabe, I. and Irwan, R. The role Hubbard and Spin-Orbit Coupling in Electronic Properties of Eu₂Ir₂O₇, *Poster presentation at 6th International Conference on functional Material Science 2022 (ICFMS 2022)*. Bali, Indonesia.
2. Charoenphon, S., Reunchan P., and Watanabe I. (August, 2022). Density Functional Theory Calculations with Different Electronic Correlational Functionals Applied to La₂CuO₄. *Poster presentation at the 29th International Conference on Low Temperature Physics (LT29)*. Sapporo, Japan.
3. Charoenphon, S., Reunchan P., and Watanabe I. (August-October, 2022). DFT Investigations on Magnetic Properties and Muon Position in La₂CuO₄ by Using LSDA+U Functional. *Poster presentation at the 15th International Conference on Muon Spin Rotation, Relaxation and Resonance (MuSR2022)*. Science and Technology Campus, University of Parma, Parma, Italy.
4. Charoenphon, S., Reunchan P., and Watanabe I. (November, 2022). Density Functional Theory Calculations with Different Electronic Correlational Functionals Applied to La₂CuO₄. *Poster presentation at the Asia-Pacific Condensed Matter Physics Conference (AC2MP2022)*. Tohoku University, Sendai, Japan.